Int. Journal of Refractory Metals and Hard Materials 56 (2016) 8–17

Contents lists available at ScienceDirect

Int. Journal of Refractory Metals and Hard Materials

journal homepage: www.elsevier.com/locate/IJRMHM

Effect of hot rolling and annealing on the mechanical properties and thermal conductivity of W-0.5 wt.% TaC alloys

S. Miao [a,b], Z.M. Xie [a,b], X.D. Yang [a,b], R. Liu [a,b], R. Gao [a,b], T. Zhang [a,b,c,*], X.P. Wang [a,b], Q.F. Fang [a,b], C.S. Liu [a,b], G.N. Luo [d], X. Liu [e], Y.Y. Lian [e]

[a] Key Laboratory of Materials Physics, Institute of Solid State Physics, Chinese Academy of Sciences, Hefei 230031, China
[b] University of Science and Technology of China, Hefei 230026, China
[c] Hefei Science Center, Chinese Academy of Sciences, Hefei, China
[d] Institute of Plasma Physics, Chinese Academy of Sciences, Hefei 230031, China
[e] Southwestern Institute of Physics, Chengdu, China

ARTICLE INFO

Article history:
Received 28 September 2015
Received in revised form 24 November 2015
Accepted 11 December 2015
Available online 15 December 2015

Keywords:
W–TaC alloys
Hot rolling and annealing
Mechanic properties
Thermal conductivity

ABSTRACT

The mechanical properties and thermal conductivity of W-0.5 wt.% TaC alloys prepared by spark plasma sintering as well as ordinary sintering followed by hot rolling and annealing treatment, respectively, were investigated. Tensile tests indicate that below 600 °C there is no tensile plastic deformation while at 700 °C the total elongation of spark plasma sintered (SPSed) W-0.5 wt.% TaC is up to 36%, which is about 3.3 times that of spark plasma sintered W samples. In contrast, the tensile strength and total elongation of rolled W-0.5 wt.% TaC are 717 MPa and 10.7% at 250 °C, respectively. The ductile-brittle transition temperature (DBTT) of rolled W-0.5 wt.% TaC is between 200 °C and 250 °C, about 300 °C lower than that of spark plasma sintered W-0.5 wt.% TaC (~600 °C). Annealing decreases the DBTT (~200 °C) and improves thermal conductivity from 175 to 186 W/m·K at room temperature. Microstructure analyses indicates that TaC could purify and strengthen grain boundaries by capturing impurity oxygen in tungsten to form Ta_2O_5. The results indicate that strength, ductility and thermal conductivity can be improved by purifying, hot rolling and subsequent annealing.

1. Introduction

Tungsten materials have been attracting growing interest as a promising candidate for plasma facing materials (PFMs) based on its high melting point, high temperature strength, and good thermal conductivity as well as its low erosion in fusion radiation environment and low tritium retention [1–3]. It offers an advantageous characteristic with regard to other potential PFMs. However, the inherent disadvantages of pure tungsten materials, including poor low temperature machinability, low ductility, high ductile-brittle transition temperature (DBTT) of about 800 °C [4] and irradiation-induced embrittlement, cannot be ignored for fusion reactor application, which is directly correlated to material's low ductility and low grain boundary (GB) strength [5]. In the PFMs' application field, low ductility, low strength and radiation induced embrittlement are the main concerns.

In recent studies, some process strategies focus on manufacturing nanostructured tungsten materials through dispersing oxide nanoparticles into W matrix [6,7]. The addition of rare earth oxides such as La_2O_3 and Y_2O_3 processed by powder metallurgy methods can effectively inhibit grain growth and thus reduce grain size. Meanwhile these oxide dispersion strengthened (ODS) W alloys are effective in stabilizing microstructures at high temperature and enhancing strength by nanosized oxide particles pining dislocations and GBs [7]. However, the ductility of these ODS-W materials is still not good. For example, W-La_2O_3 exhibits DBTT higher than 400 °C [8]. W-Y_2O_3 alloys cannot keep thermal stability owing to the coarsening of oxide particle at elevated process temperature (above 2000 °C). Recently, W-1.1% TiC alloys with ultrafine grains fabricated by super plastic deformation exhibit very high fracture strength up to about 4.4 GPa and appreciable bend ductility at RT [9,10]. However, the inferior fabrication efficiency, economy and the limited size of W-1.1% TiC alloys make it unsuitable for preparing large scale PFMs or diverters.

In comparison with the compounds of Y_2O_3 (2410 °C), La_2O_3 (2217 °C) and TiC (3067 °C), tantalum carbide (TaC) with a relatively higher melting point (3880 °C) and good thermal stability can enhance the erosion resistance of W alloys [11,12]. Moreover, it is also found that Ta is a more suitable alloying element because of its good resistance to H and D-retention under high density plasma irradiation at

* Corresponding author at: University of Science and Technology of China, Hefei 230026, China.

http://dx.doi.org/10.1016/j.ijrmhm.2015.12.004
0263-4368/

Table 1
Chemical composition of the as received tungsten powders and TaC powders (wt.%).

	Cr	Ti	Fe	O	C	P	S	N	W
W Powder	0.005	0.005	0.001	0.24	0.0029	0.0005	0.0005	–	Bal
	Nb	Ti	Fe	O	C	K	Ca	N	Si	Na	Ta
TaC Powder	0.05	0.01	0.05	0.71	8.20	0.05	0.01	0.01	0.01	0.01	Bal

high temperature [13]. These superior performances make TaC very attractive in the strengthening of tungsten materials. However, there is very few data reported about the mechanical and thermal properties of W-TaC alloys.

As well known, low temperature mechanical properties of W highly depend on the purity and work processing. The fabrication routes and thermo-mechanical treatment reveal a significant influence on the mechanical properties and DBTT of W [14,15]. In this work, W-0.2, -0.5, -0.8 and -1.0 wt.% TaC alloys were fabricated by different consolidation methods (i.e., spark plasma sintering technique (SPS) and conventional sintering) following thermo-mechanical treatment (for hot rolled W-0.5% TaC). The effects of different amounts of TaC and working processes on mechanical properties, microstructure and thermal conductivity were investigated.

2. Experimental details

2.1. Starting materials, ball milling method and fabrication route

Pure W and W-0.2, -0.5, -0.8 and -1.0 wt.% TaC alloys (hereafter abbreviated as WTC02, WTC05, WTC08 and WTC10, respectively) were fabricated using pure W (purity >99.9% trace metal basis, the chemical content of tungsten powder was listed in Table 1.) and nanosized TaC powders (average particle diameter 100 nm, purity >99.5%, the chemical content of TaC powder was listed in Table 1.). Powders were ball-milled in a planetary ball mill machine for 4 h in argon atmosphere (oxygen (O) < 0.1 ppm, H_2O < 0.1 ppm) with ball-to-powder weight ratio of 8:1 and a rotation speed of 240 rpm. Tungsten carbide balls and mortars were used to minimize the possible impurity contamination. The consolidation of the samples (WTC02, WTC05, WTC08 and WTC10) was carried out through spark plasma sintering (SPS, furnace SE-607, FCT Group, Germany) technique. All of the samples were SPSed following the same sintering program described elsewhere [16]. The size of SPSed samples is 20 mm in diameter and about 2.0 mm in thickness. In order to study the hot rolling effect, WTC05 alloys were fabricated by collaborating with Beijing Qianlong Tungsten & Molybdenum Co., Ltd. First, the same ball-milled WTC05 powders were sintered at 2300 °C for 4 h. Subsequently, sintered billets were hot rolled into 7 mm from original thickness of ~23 mm. Fig. 1 shows the detailed process flow diagram. The hot rolled samples for tensile test were sectioned along the rolling direction and the specimens for metallographic investigation were cut on the rolling direction (RD)–normal direction (ND) and RD–transverse direction (TD) surface.

2.2. Relative density, tensile tests, microstructure and thermal conductivity

Density of the sintered samples was determined by Archimedes principle. Theoretical density of the samples was calculated from the fraction and density of each component. Densities of tungsten and TaC were taken as 19.35 g/cm^3 and 14.3 g/cm^3, respectively. For tensile testing, all SPSed and hot rolled samples were cut and polished into dog-

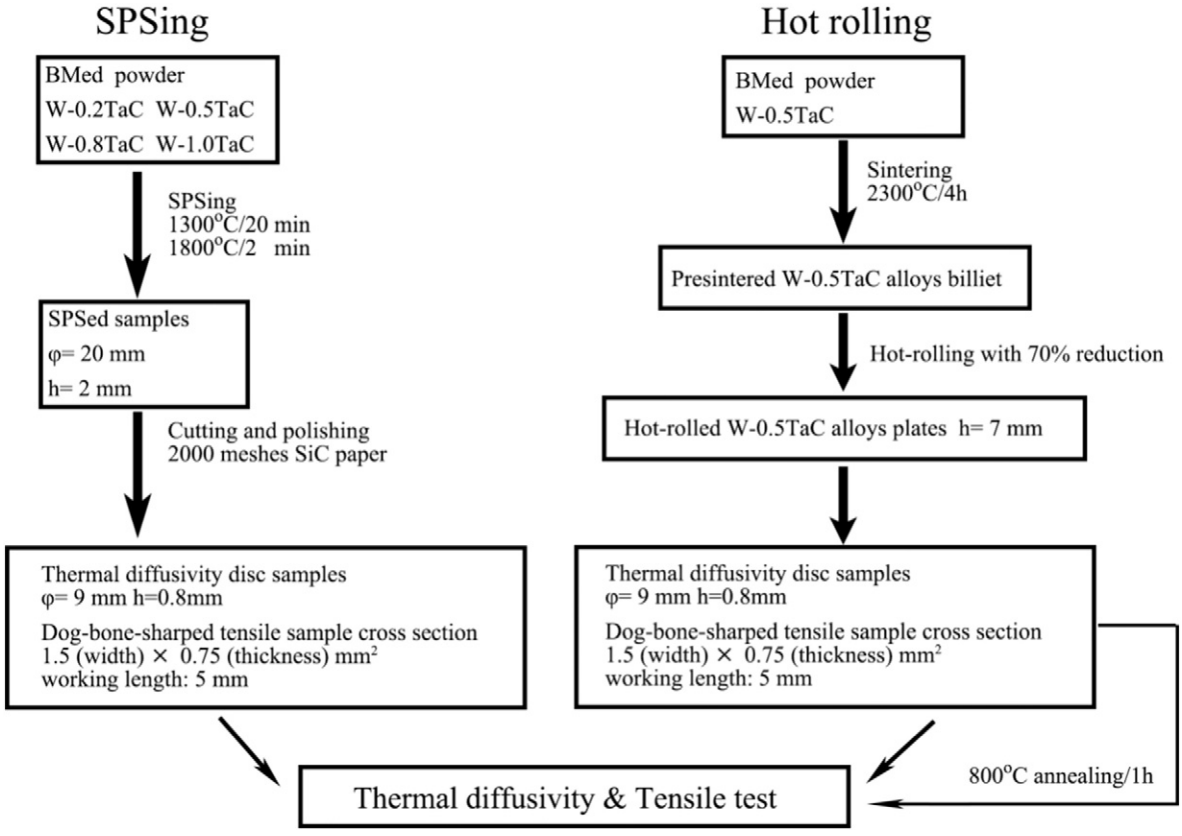

Fig. 1. A sketch of working processes.

bone-shaped samples with a cross section of 1.5 × .75 mm^2 and a working length of 5 mm, as shown in Fig. 2. The tensile tests were carried out at various temperatures from room temperature (RT) to 700 °C in Ar atmosphere, using an Instron-5967 machine at a constant speed of 0.06 mm/min. Tensile strength and total elongation were deduced from the stress–strain curves and total elongations were determined by measuring the length of fractured samples using vernier caliper.

The samples for metallography were prepared by polishing and etching sample surfaces (etching solution: 10% potassium ferricyanide with 10% sodium hydroxide aqueous solution). The average grain size of W was measured based on over 300 grains in different optical microscope (OM, ZEISS–AX10) graphs. Fracture surfaces of SPSed and rolled WTC05 samples after destructive tensile testing were characterized by field emission scanning electron microscope (FESEM Sirion 200, FEI). Transmission electron microscope (TEM, JEM–2000FX) was used to study the microstructure of samples. Energy-dispersive X-ray spectroscopy (EDS, INCA) analytical system installed on TEM was used for elemental analyses.

Thermal diffusivity (α) was measured by the laser flash diffusivity system (LFA457 Micro flash, NETZSCH). The thermal conductivity (γ) was calculated from thermal diffusivity (α), density (ρ), to specific heat (C_p) according to the equation $\gamma = \alpha \cdot C_p \cdot \rho$. The specific heat data was adopted from Ref. [17].

3. Results and discussions

In order to investigate the influence of TaC content on the microstructure and mechanical properties of W-TaC alloys, pure W and W-0.2, -0.5, -0.8 and -1.0 wt.% TaC alloys were prepared using SPS technique. Density of SPSed pure W and W-TaC alloys was plotted as the TaC content in Fig. 3. All SPSed samples are well consolidated. With increasing TaC content, the density of SPSed specimen increases up to 99.2% for WTC05, as listed in Table 2. However, the relative density decreases with further increasing TaC content from 0.5% to 1.0%. Metallographic analyses indicates that tungsten grains have spherical shape with the dimension ranging from 3.42 to 4.65 μm and average grain size of 4.12 μm in SPSed pure W. While the diameters of tungsten grain of SPSed W-TaC samples are in the range from 3.42 to 3.65 μm (with average size ~3.5 μm). That is to

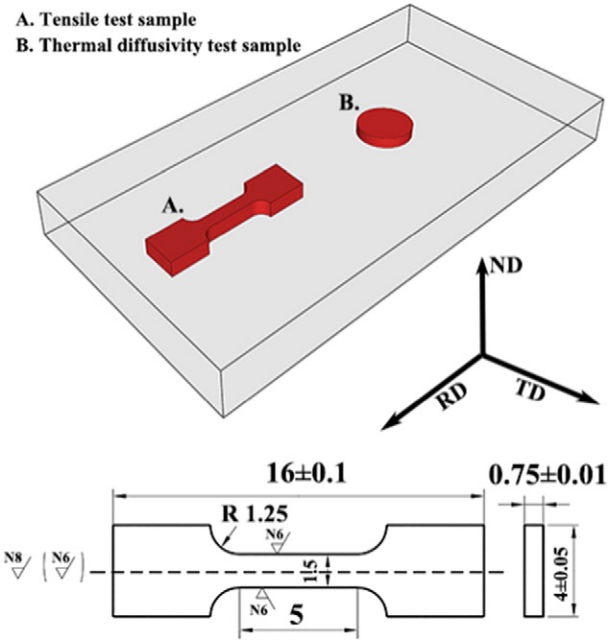

Fig. 2. Geometry and dimensions of tensile and thermal conductivity test samples.

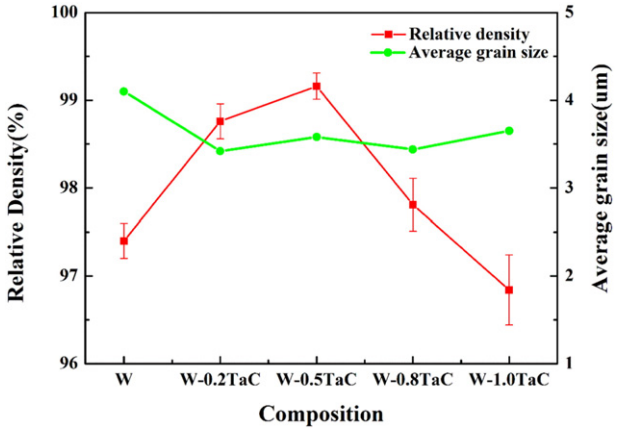

Fig. 3. Average grain size and relative density of SPSed samples.

say, trace TaC could inhibit the growth of tungsten grain during high temperature SPS process. Tungsten grains in hot rolled WTC05 samples have near equiaxed structure with grain sizes ranging from 107 to 130 μm in RD (average size ~116 μm), 100 to 120 μm in TD (average size ~108 μm) and 90 to 105 μm in ND (average size ~94 μm), as shown in Fig. 4c and d. The grain dimension of annealed samples changed slightly as shown in Fig. 4e. These results may come from the recrystallization during rolling process resulted from relatively high rolling temperature (1600 °C), which is different from that of the warm rolled tungsten [18].

The engineering stress–strain curves of SPSed W and WTC05 at various temperatures are presented in Fig. 5a with the correction of machine compliance. The ultimate tensile strength (UTS) and total elongation (TE) of these SPSed samples at various temperatures are listed in Table 3 and presented in Fig. 6. The SPSed W shows typical brittle fracture at 600 °C with a fracture strength of 279 MPa, indicating a DBTT higher than 600 °C. The SPSed WTC02 (with 0.2 wt.% TaC addition) samples exhibit tensile deformation at 650 °C with TE ~5.5% but fail in elastic region at 600 °C, while the TE of SPSed WTC05 reaches up to 40.0% at 600 °C as shown in Fig. 5a, which is markedly larger than that of all previously reported SPSed tungsten materials [6,16], indicating an unprecedented tensile ductility/plasticity of SPSed WTC05 (DBTT < 600 °C) at 600 °C. However, with further increasing TaC content, tensile properties of SPSed WTC08 and WTC10 samples degrade unpredictably as they are typically brittle at 700 °C (where pure W is ductile with TE ~11%). These results indicate that an appropriate TaC content could increase the tensile properties of SPSed W-TaC alloys reducing DBTT and the 0.5 wt.% TaC is the best.

It is well known that the rolling process could further improve low temperature toughness and reduce DBTT. Though rolled WTC05 samples show typical brittle fracture at 200 °C with an elongation of only 0.7%, the UTS reaches up to 600 MPa as shown in Fig. 5b. At 250 °C, the rolled WTC05 shows obvious plasticity along RD with TE of ~10%

Table 2
Working process, composition, density, and average grain size of W-TaC alloys.

Working process	Composition (wt.%)	Density/relative density (g/cm^3)/(%)	Average grain size (μm)
SPS	W	18.80/97.4	4.1
SPS	W-0.2 TaC	18.98/98.76	3.42
SPS	W-0.5 TaC	19.05/99.16	3.58
SPS	W-0.8 TaC	18.77/97.81	3.44
SPS	W-1.0 TaC	18.57/96.84	3.65
Hot rolling	W-0.5 TaC	19.13/99.6	R 116.7 L 113
Hot rolling + annealing	W-0.5 TaC	19.14/99.7	R 103.4 L 124

and UTS of ~717 MPa, indicating that the DBTT of rolled WTC05 is between 200 °C and 250 °C, which is 300 °C lower than that of SPSed WTC05 and rolled WL10 and W-K [19]. Furthermore, the UTS of rolled WTC05 is always larger than that of other SPSed W-TaC samples at various temperatures, as shown in Fig. 5b. As compared with SPSed WTC05 sample, the TE of rolled WTC05 at 600 °C is smaller, while the tensile strength of rolled WTC05 is 80 MPa larger than that of SPSed WTC05. The reduced plastic deformation may result from an increasing W grain size (above 100 μm) induced by recrystallization in rolled WTC05. The enhancing tensile strength benefits from strengthened grain boundaries and W/Ta phase boundaries during the hot rolling process, which will be discussed later in detail.

The rolled WTC05 was annealed at 800 °C for 1 h, in order to investigate annealing effect on the mechanical properties. The DBTT region of rolled WTC05 is reduced by about 50 °C after 800 °C annealing for 1 h (hereafter abbreviated an annealed one as A-rolled WTC05, see Fig. 5b). The TE of A-rolled WTC05 is 5.2% at 200 °C, which is 7.4 times that of the unannealed one. This significant increase in low temperature ductility can be attributed to the elimination of residual stress and point defects in rolled WTC05 during annealing process. The UTS of A-rolled WTC05 keeps about 450 MPa from RT to 600 °C and does not change distinctly compared to the unannealed one, as presented in Fig. 5b. It can be concluded that annealing treatment at 800 °C enhances the mechanical properties (i.e., increasing low temperature plasticity and reducing the DBTT) of hot rolled tungsten alloys.

Fig. 7 shows the SEM micrographs of tensile fracture surfaces of the as received tungsten, SPSed WTC05 and rolled WTC05. As shown in Fig. 7a and b, the fracture surface of SPSed W (Fig. 7a) contains an overwhelming majority of intergranular rupture (94.66%) and few transgranular rupture (5.34%). Meanwhile SPSed W samples exhibit some residual pores, which significantly weaken the strength. While SPSed WTC05 (Fig. 7b) samples exhibit less residual pores compared with SPSed W with increased transgranular ruptures (26.5%), which is attributed to strengthened tungsten GBs by TaC addition. The rolling process can obviously eliminate porosity by plastic deformation and thus lead to a nearly full dense bulk W-0.5 wt.% TaC alloy with a

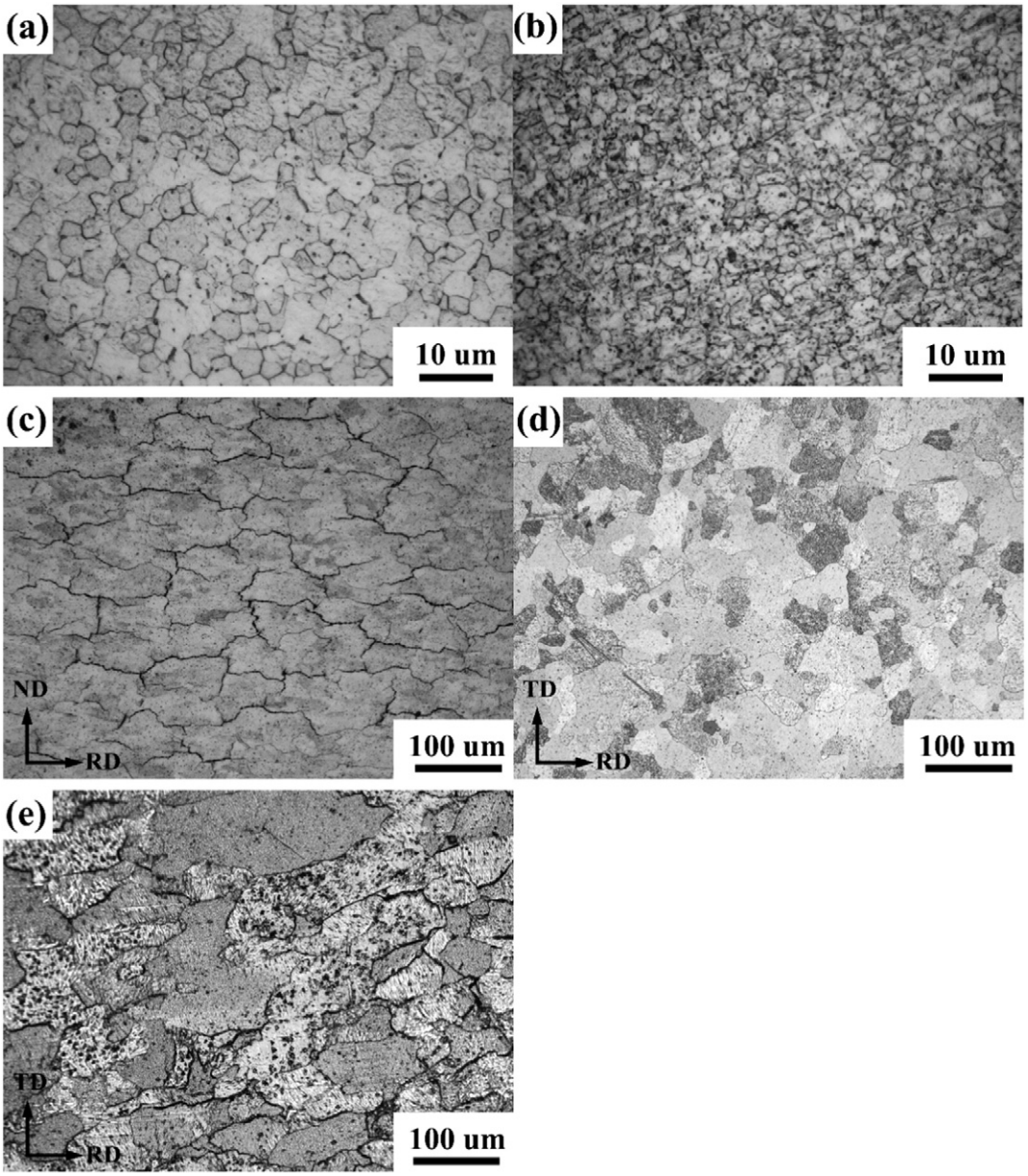

Fig. 4. Optical micrographs of the as SPSed W (a) and WTC05 (b),ND–RD surface of rolled WTC05(c), TD–RD surface of rolled WTC05 (d) and TD–RD surface of A-rolled WTC05 (e).

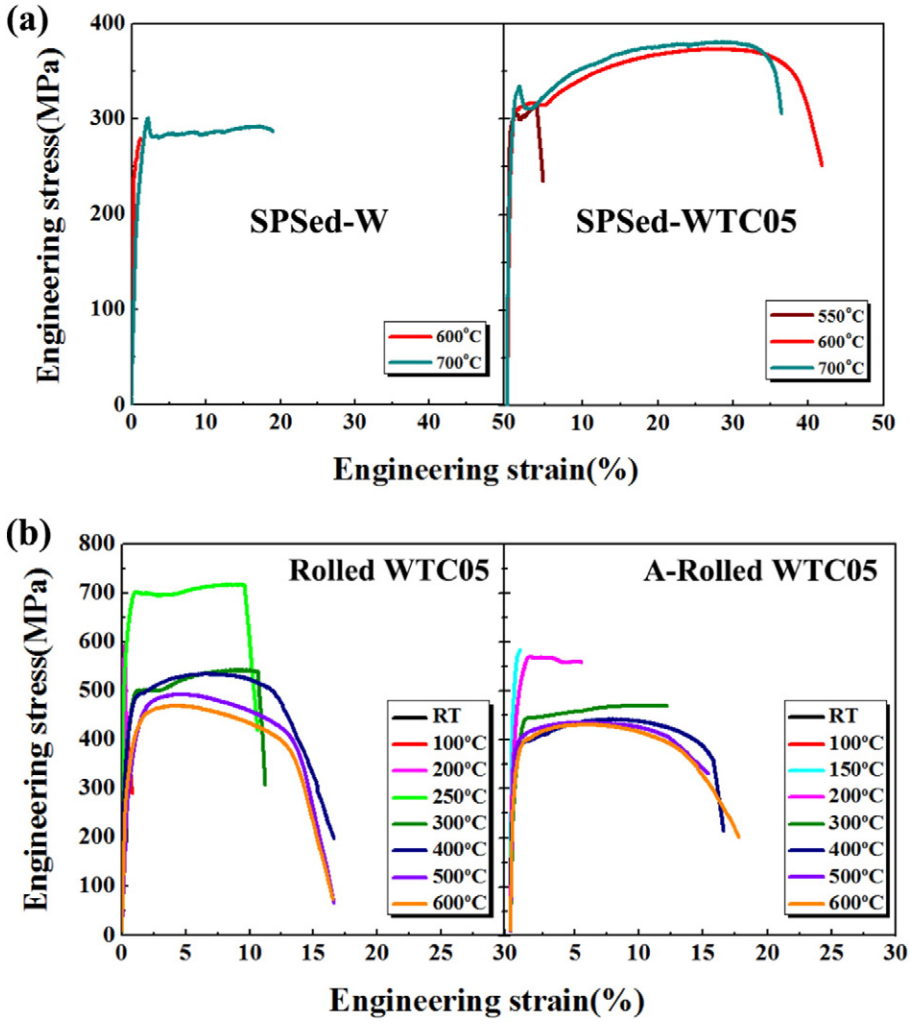

Fig. 5. Tensile behavior of as SPSed W (a), WTC05 (a), rolled WTC05 (b) and A-Rolled WTC05 (b) alloys at various temperatures.

corresponding result of almost 100% transgranular fractures (Fig. 7c) in rolled samples. These different fracture features give a reasonable explanation for the increased strength of rolled WTC05. Fig. 7d depicts the tensile fracture morphology of rolled WTC05 at 300 °C. The plastic deformation and delamination structures caused by stress during tensile test are clearly seen, which is completely different from the RT fracture morphology.

The microstructure is closely related to the mechanical properties. Therefore, the effects of TaC addition on the microstructure were investigated by TEM and EDS analyses. In order to characterize the dispersion of nanosized dispersoid particles, TEM analyses is conducted, as shown in Fig. 8. The corresponding number density of dispersed particles in each SPSed sample was calculated. In SPSed WTC02 and WTC05, nanoparticles were harmoniously dispersed in tungsten grain interior or located at GBs (see Fig. 8a and b), and the particle size ranges from 30 to 400 nm with average value of 142 nm and 179 nm, respectively. In SPSed WTC08 and WTC10 samples, however, seriously clustered particles were observed and the particle sizes were mainly larger than 100 nm (see Fig. 8c and d). Especially, the area fraction of large particles (larger than 100 nm) reached 87.2% in SPSed WTC10 sample, which is 1.41 times larger than that of SPSed WTC05 (about 59%). The clustered particles were mostly located at GBs in SPSed WTC08 and WTC10 samples, which may introduce stress concentrations and become the possible sites of crack initiation. Therefore, the tensile properties of SPSed WTC08 and WTC10 were worse than that of SPSed WTC05. As presented in Fig. 9, representative TEM images of rolled WTC05 alloys revealed that nanosized particles were both homogeneously dispersed in the matrix and partially located at the GBs, which was similar to that of the SPSed one. Dispersed particles in the grain's interior could effectively pin dislocation, which would enhance work hardening and sustain uniform elongations as shown in Fig. 5a. Meanwhile, nanoparticles (<100 nm) located at GBs could hinder grain sliding and increase the high temperature strength and stability of WTC05 alloys.

To further clarify the phase of particles in rolled WTC05 sample, selected area electron diffraction (SAED), high resolution transmission electron microscopy (HRTEM) and EDS were employed. The EDS analyses of more than 50 particles in grain interior or at GBs shows that Ta and O signals are always detected and the approximate atomic ratios are about 2:5, as shown in Fig. 10a and the inset. In Fig. 10b and the inset, the SAED results reveal that these particles are crystalline with

Table 3
Tensile properties of SPSed W–TaC composites at various temperatures.

Materials	Tensile strength (MPa)/elongation (%)					
	500 °C	550 °C	600 °C	650 °C	700 °C	750 °C
W	–	–	279[a]/–	–	300/18.7%	287/8.7%
WTC02	–	262[a]/–	248[a]/–	367[a]/5.5%	360/21.2%	374/10.7%
WTC05	225[a]/–	314[a]/4.0%	371/40.0%	385/37.6%	379/36.3%	347/21.4%
WTC08	–	70[a]/–	217[a]/–	373[a]/–	373[a]/–	380/17.9%
WTC10	–	89[a]/–	186[a]/–	375[a]/–	384[a]/–	317/13.5%

[a] Brittle fracture.

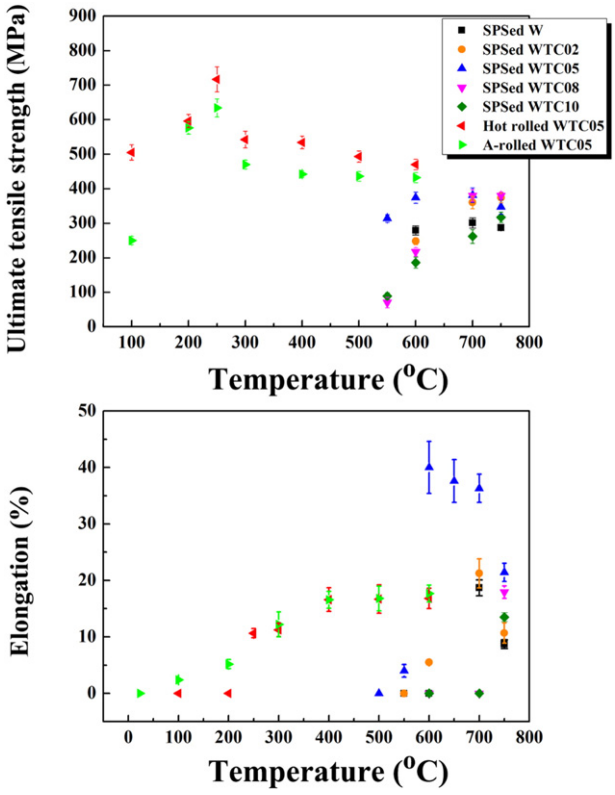

Fig. 6. The UTS and total elongation of SPSed W, SPSed WTC05, rolled WTC05, A-Rolled WTC05 alloys at different temperatures.

an orthorhombic structure. The corresponding HRTEM images clearly show two perpendicular crystalline planes with measured spaces of 0.386 nm and 0.312 nm, which match well with the value of crystalline planes of (001) and (110) in an orthorhombic Ta_2O_5 particle from Powder Diffraction File (PDF) card (reference code: 00-008-0255), respectively. The formation of Ta_2O_5 particles is most probably owing to the TaC particles capturing trace impurity oxygen in tungsten during sintering. This purification strategy would undoubtedly reduce impurity oxygen concentration in grain boundaries and thus enhance GB strength and ductility of tungsten alloys, which leads to an extraordinary tensile ductility (TE ~40%) of SPSed WTC05 at a relatively high temperature (600 °C).

As well known, the microstructural parameters (such as grain size and shape, grain boundary, defect, impurity,) play a significant role in the thermal conductivity of materials. To evaluate the influence of TaC addition and working process on the thermal conductivity of W, the thermal conductivity of SPSed W, W-TaC alloys with 0.2, 0.5, 0.8, 1.0 wt% TaC, and hot rolled W-0.5 wt.% TaC (before and after annealing) was measured and shown in Fig. 11. The thermal conductivity of SPSed W-TaC alloys increases with increasing TaC addition from 0.2 to 0.5 wt.%, and then decreases with more than 0.5 wt.% TaC addition. However, the thermal conductivity for all SPSed W-TaC samples is lower than that of SPSed W, which could result from more GB areas (smaller tungsten grain) and more W-TaC (O) phase boundaries (PBs) in SPSed W-TaC than those of SPSed W. These increasing GBs or PBs may significantly enhance the interface scattering on electrons and therefore reduce the electronic thermal conductivity of SPSed W-TaC alloys. However, in rolled WTC05 samples, the thermal conductivity along RD direction is 175 W/m·K, about 26% larger than that of SPSed W (139 W/m·K) at RT, which is attributed to large tungsten grains along the L direction with an average grain length of 126.7 μm (3.2 μm in SPSed W). The number density of GBs is significantly decreased in

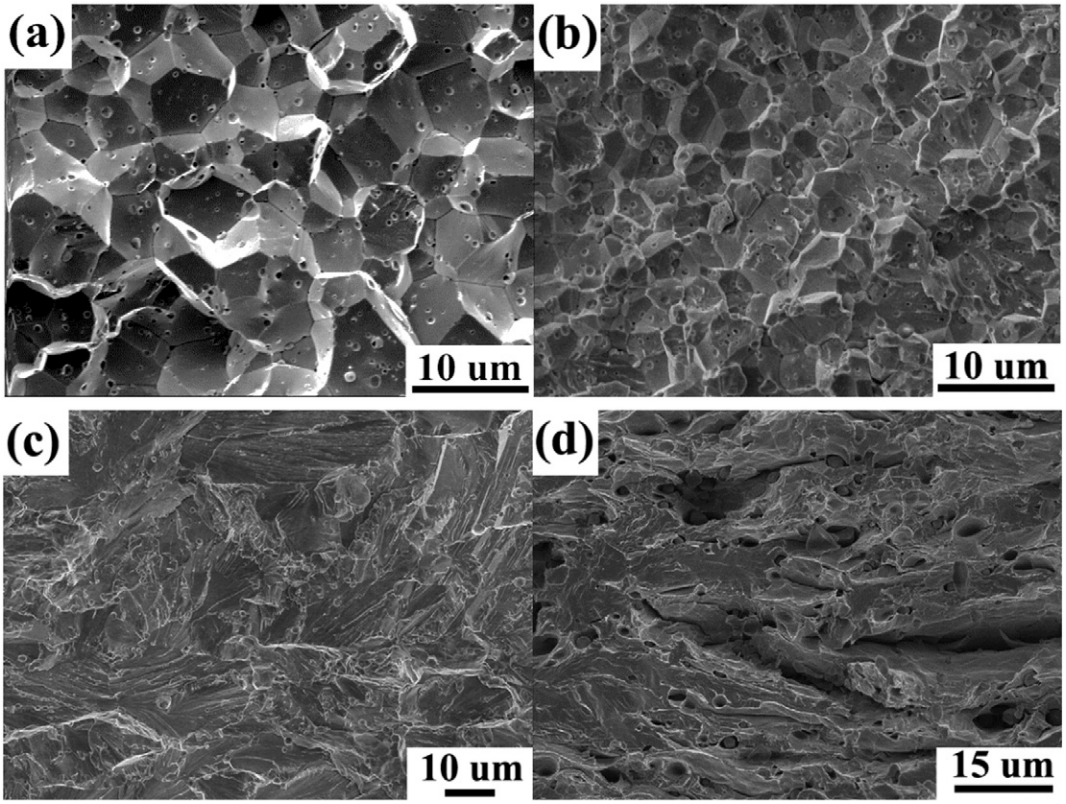

Fig. 7. SEM images of fracture surfaces of SPSed W at RT (a), SPSed WTC05 at RT (b), rolled WTC05 at RT(c) and rolled WTC05 at 300 °C (d).

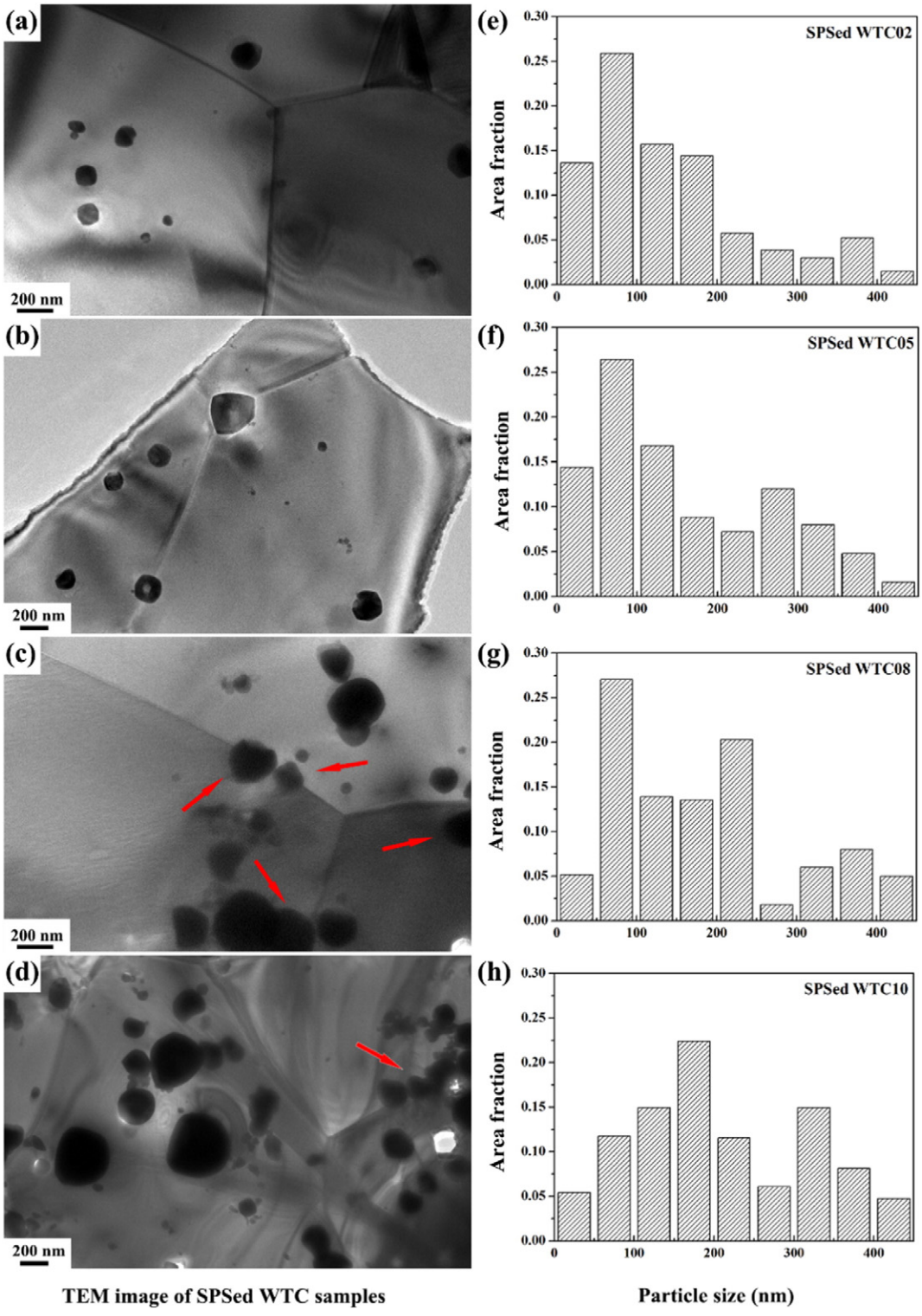

Fig. 8. TEM micrographs (left) of SPSed WTC02 (a), WTC05 (b), WTC08 (c), and WTC10 (d) and the corresponding grain size distribution of the dispersed particles (right) in SPSed WTC02 (e), WTC05 (f), WTC08 (g), and WTC10 (h).

rolled WTC05 which weakens the interface scattering on electrons and thereby enhances the thermal conductivity. After 800 °C annealing for 1 h, the thermal conductivity of A-rolled WTC05 is larger than 124 W/m·K below 500 °C, which is slightly higher than that of the unannealed one. And at RT, the thermal conductivity of A-rolled WTC05 is even as high as 186 W/m·K, which is beyond the level of ITER grade tungsten materials (~174 W/m·K) [20]. It is known that annealing process eliminating point defects and dislocations would reduce electron scattering and thus improve the electron thermal conductivity [21].

4. Conclusions

W-TaC alloys with 0, 0.2, 0.5, 0.8 and 1.0 wt.% TaC were fabricated by SPS sintering and hot rolling process. The grain size of SPSed WTC alloys

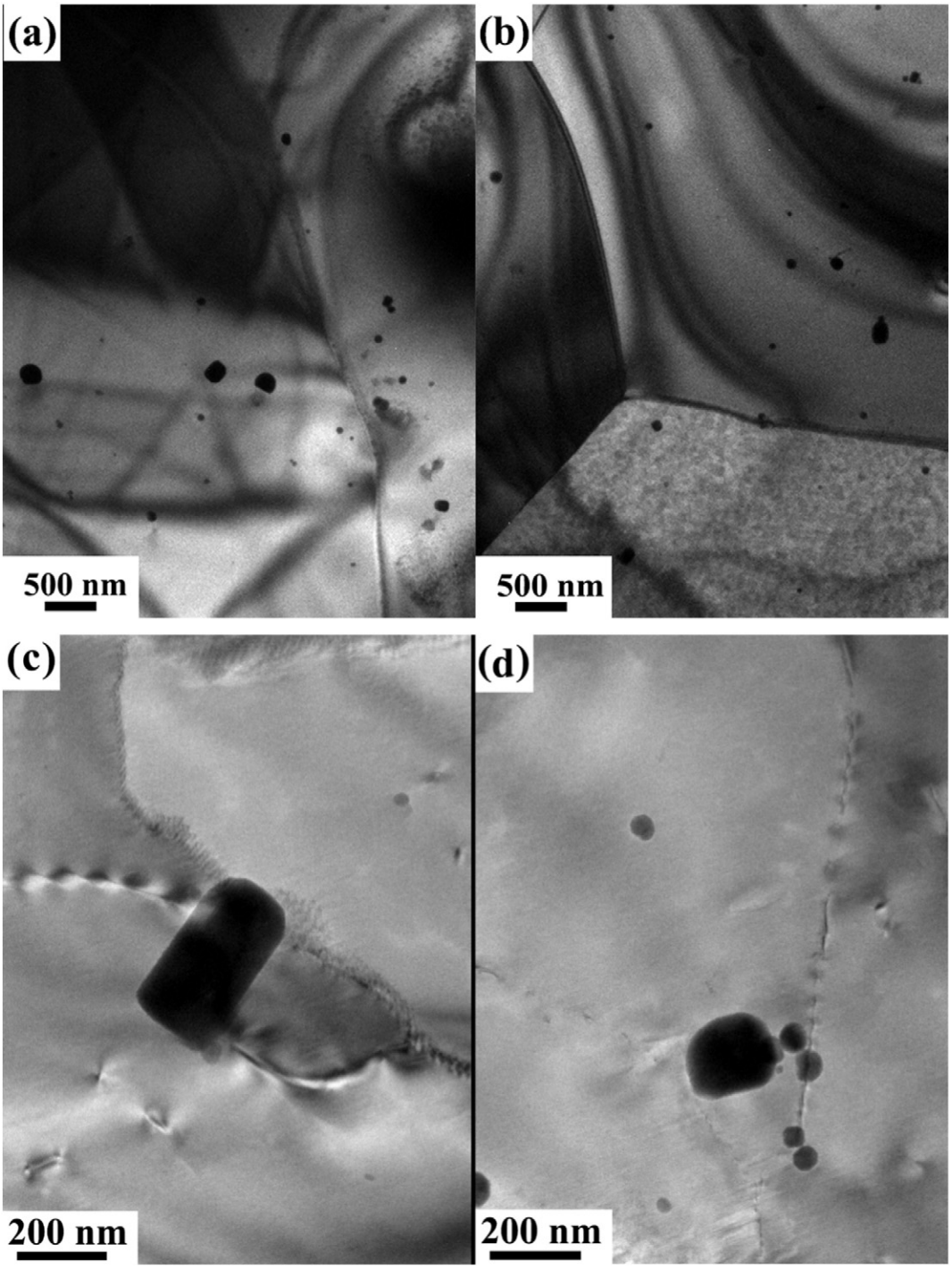

Fig. 9. TEM micrographs of rolled WTC05 (a) and (b), pinning dislocation (c) and (d).

ranges from 3.42 to 3.65 μm. The mechanical properties, the microstructures and the thermal conductivity were studied.

1. According to the evolution of mechanical properties, 0.5 wt.% TaC content was chosen as the optimizing composition.
2. The DBTT value for rolled WTC05 is between 200 °C and 250 °C, much lower than that of SPSed WTC05 (~600 °C). The total elongation and UTS of rolled WTC05 at 250 °C are 10.7% and 717 MPa, respectively.
3. In rolled WTC05 samples, tungsten grains possess nearly equiaxed structures with an average diameter of ~100 μm and Ta_2O_5 particles with an average particle size of 179 nm are homogeneously dispersed in the matrix or located at GBs.
4. The thermal conductivity of A-rolled WTC05 (186 W/m·K) is much larger (about 60% larger) than that of SPSed WTC05 and reaches the level of ITER grade tungsten materials.
5. TaC reacts with impurities of oxygen in W to form Ta_2O_5, reducing oxygen concentration at grain boundaries and thus enhancing grain boundary strength and the ductility of tungsten materials.

Acknowledgments

This work was financially supported by the National Magnetic Confinement Fusion Program (Grant No. 2015GB112000), the National Natural Science Foundation of China (Grant Nos. 11575241, 11374299,

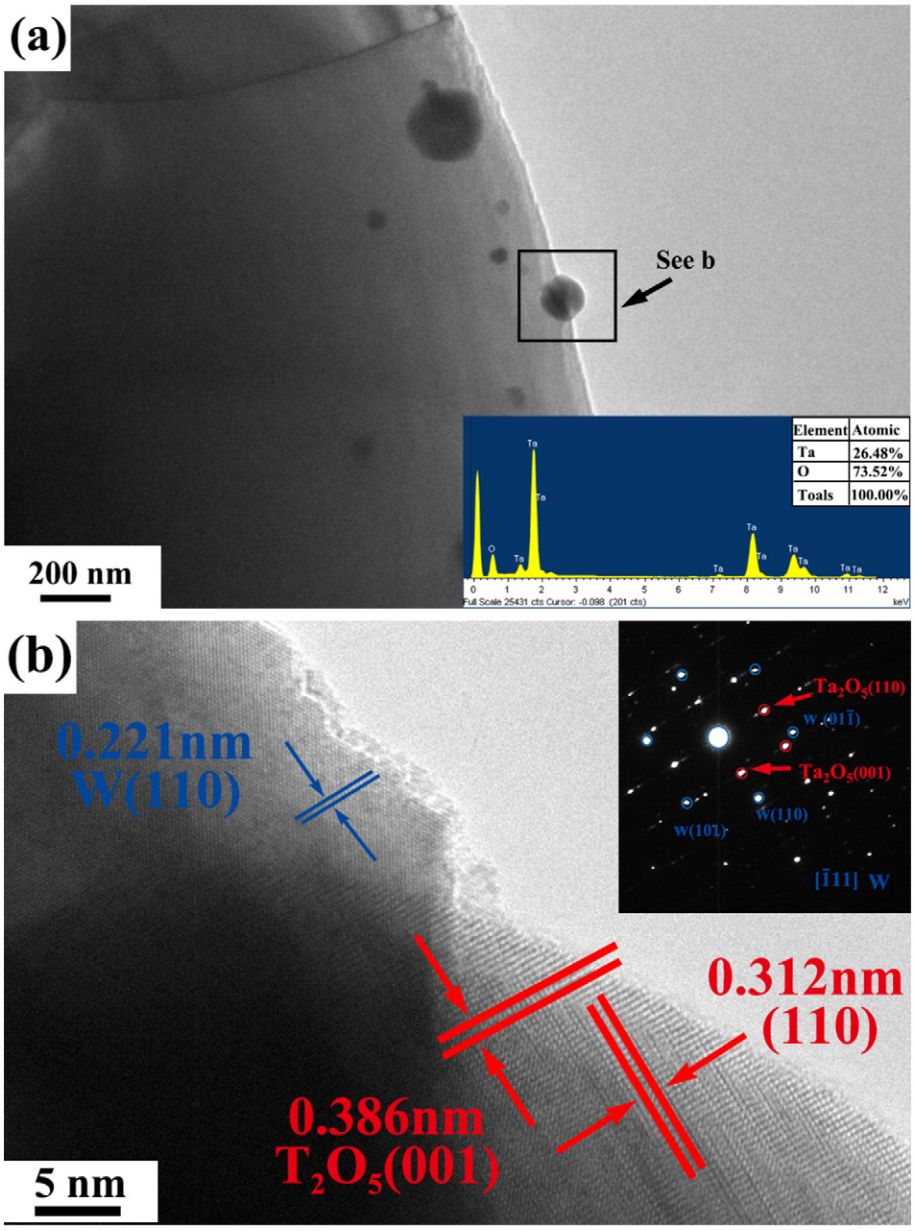

Fig. 10. The EDS results of dispersed particles (a) and (b) the high resolution transmission electron microscopy and selected area electron diffraction (SAED).

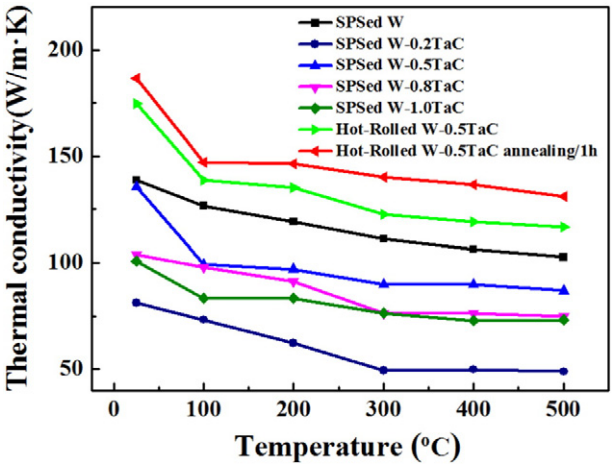

Fig. 11. Comparison of thermal conductivity of SPSed W and WTC02, WTC05, WTC08, WTC10, rolled WTC05 and A-rolled WTC05.

11301164, 11375230, 11274305, 11475216), Users with Potential (2015HSC-UP005) and Anhui provincial Natural Science Foundation of China (Grant No. 1408085QE77).

References

[1] P. Norajitra, L.V. Boccaccini, E. Diegele, V. Filatov, A. Gervash, R. Giniyatulin, S. Gordeev, V. Heinzel, G. Janeschitz, J. Konys, W. Krauss, R. Kruessmann, S. Malang, I. Mazul, A. Moeslang, C. Petersen, G. Reimann, M. Rieth, G. Rizzi, M. Rumyantsev, R. Ruprecht, V. Slobodtchouk, J. Nucl, Mater. 329-333 (2004) 1594–1598.
[2] G.A. Cottrell, Mater. Sci. Technol. 22 (8) (2006) 869–880.
[3] P. Norajitra, L.V. Boccaccini, A. Gervash, R. Giniyatulin, N. Holstein, T. Ihli, G. Janeschitz, W. Krauss, R. Kruessmann, V. Kuznetsov, A. Makhankov, I. Mazul, A. Moeslang, I. Ovchinnikov, M. Rieth, B. Zeep, J. Nucl. Mater. 367-370 (2007) 1416–1421.
[4] D. Stork, P. Agostini, J.L. Boutard, et al., J. Nucl. Mater. 455 (2014) 277–291.
[5] G. Pintsuk, 4.17-Tungsten as a plasma-facing material, in: R.J.M. Konings (Ed.), Comprehensive Nuclear Materials, Elsevier, Oxford 2012, pp. 551–581.
[6] R. Liu, Y. Zhou, T. Hao, T. Zhang, X.P. Wang, C.S. Liu, Q.F. Fang, J. Nucl. Mater. 424 (2012) 171–175.
[7] M. Battabyal, R. Schäublin, P. Spätig, M. Walter, M. Rieth, N. Baluc, J. Nucl. Mater. 442 (2013) S225–S228.
[8] I. Smid, M. Akiba, G. Vieider, L. Plöchl, J. Nucl. Mater. 258–263 (1998) 160–172.

[9] H. Kurishita, S. Matsuo, H. Arakawa, S. Kobayashi, K. Nakai, T. Takida, K. Takebe, M. Kawai, Mater. Sci. Eng. A 477 (2008) 162–167.
[10] M. Kajioka, T. Sakamoto, K. Nakai, S. Kobayashi, H. Kurishita, S. Matsuo, H. Arakawa, J. Nucl. Mater. 417 (2011) 512–515.
[11] Y. Ueda, M. Oya, Y. Hamaji, H.T. Lee, H. Kurishita, Y. Torikai, et al., Phys. Scr. T159 (2014) 014038.
[12] M. Oya, H.T. Lee, Y. Ohtsuka, Y. Ueda, H. Kurishita, M. Oyaidzuand, T. Yamanishi, Phys. Scr. T159 (2014) 014048.
[13] H. Kurishita, S. Matsuo, H. Arakawa, T. Sakamoto, S. Kobayashi, K. Nakai, H. Okano, H. Watanabe, N. Yoshida, Y. Torikai, Y. Hatano, T. Takida, M. Kato, A. Ikegaya, Y. Ueda, M. Hatakeyama, T. Shikama, Phys. Scr. T159 (2014) 014032.
[14] A. Wronski, A. Foukdeux, J. Less-Common. Met. 8 (1965) 149–158.
[15] I. Smid, M. Akiba, G. Vieider, L. Plochl, J. Nucl. Mater. 258-263 (1998) 160–172.
[16] R. Liu, Z.M. Xie, T. Hao, Y. Zhou, X.P. Wang, Q.F. Fang, C.S. Liu, J. Nucl. Mater. 451 (2014) 35–39.
[17] I. Barin, Thermochemical Data of Pure Substances, third ed. Wiley-VCH, Verlag, GmbH, Weinheim, 1995.
[18] Q. Yan, X. Zhang, T. Wang, C. Yang, C. Ge, J. Nucl. Mater. 442 (2013) S233–S236.
[19] X. Shu, H. Qiu, B. Huang, Z. Gu, J. Yang, J. Liao, Y. Yang, N. Liu, J. Tang, J. Nucl. Mater. 440 (2013) 414–419.
[20] N. Ohno, S. Kajita, D. Nashijima, S. Takamura, J. Nucl. Mater. 363-365 (2007) 1153–1159.
[21] O.V. Ogorodnikova, J. Roth, M. Mayer, J. Nucl. Mater. 313-316 (2003) 469–477.